第38卷第7期
2022年7月

无 机 化 学 学 报
CHINESE JOURNAL OF INORGANIC CHEMISTRY

Vol.38 No.7
1402-1410

镁掺杂氧化铈整体式催化剂催化CO_2和CH_3OH直接合成碳酸二甲酯

严栎颖[1] 李 月[1] 邓 杰[1] 赵 翕[1] 塔 娜*[,2] 陈永东*[,1]

([1]西南石油大学化学化工学院,成都 610500)

([2]中国科学院大连化学物理研究所催化基础国家重点实验室,大连 116023)

摘要: 采用共沉淀法成功地合成了不同Mg掺杂量的$Ce_{1-x}Mg_xO_2$(x=0.05、0.10、0.15、0.20)固溶体催化材料,并运用透射电子显微镜(TEM)、X射线衍射(XRD)、氮气吸附-脱附测试、拉曼光谱、X射线光电子能谱(XPS)、CO_2程序升温脱附(CO_2-TPD)等技术对这些材料进行了表征。结果发现,通过调控CeO_2晶格中Mg的含量,可以调控所制备的$Ce_{1-x}Mg_xO_2$催化材料的粒径、比表面积、表面缺陷等。其中$Ce_{0.90}Mg_{0.10}O_2$展现了最佳的表面性质,具有最小的平均粒径(约5.8 nm),最大的比表面积(约136 $m^2\cdot g^{-1}$)以及最高的表面氧含量(31.98%)。将$Ce_{1-x}Mg_xO_2$催化材料涂覆在堇青石蜂窝陶瓷上制成整体催化剂,考察其对CO_2和CH_3OH直接合成碳酸二甲酯的催化性能。在140 ℃、2.4 MPa、反应2 h的条件下,$Ce_{0.90}Mg_{0.10}O_2$整体催化剂上碳酸二甲酯的收率高达20.21%,催化效果明显优于CeO_2和其余的$Ce_{1-x}Mg_xO_2$(x=0.05、0.15、0.20)催化材料。

关键词: CO_2转化;碳酸二甲酯;氧空位;整体式催化剂;铈镁复合氧化物

中图分类号: O643.32+2 **文献标识码:** A **文章编号:** 1001-4861(2022)07-1402-09

DOI: 10.11862/CJIC.2022.139

Direct Synthesis of Dimethyl Carbonate from CO_2 and Methanol by Mg-Doped Ceria Monolithic Catalyst

YAN Yue-Ying[1] LI Yue[1] DENG Jie[1] ZHAO Xi[1] TA Na*[,2] CHEN Yong-Dong*[,1]

([1]*College of Chemistry and Chemical Engineering, Southwest Petroleum University, Chengdu* 610500, *China*)

([2]*State Key Laboratory of Catalysis, Dalian Institute of Chemical Physics, Chinese Academy of Sciences, Dalian, Liaoning* 116023, *China*)

Abstract: In this paper, $Ce_{1-x}Mg_xO_2$ (x=0.05, 0.10, 0.15, 0.20) solid solution catalytic materials with different molar ratios were successfully synthesized by co-precipitation method. These materials were characterized by transmission electron microscope (TEM), X-ray diffraction (XRD), nitrogen adsorption-desorption test, Raman spectroscopy, X-ray photoelectron spectroscopy (XPS), CO_2 temperature-programmed desorption (CO_2-TPD) and other techniques. It was found that the particle size, specific surface area, surface defects, *etc*. of the prepared $Ce_{1-x}Mg_xO_2$ catalytic materials can be tuned by regulating the content of Mg in the CeO_2 lattice. Among them, $Ce_{0.90}Mg_{0.10}O_2$ exhibited the best surface properties, with the smallest average particle size of about 5.8 nm, the largest specific surface area of about 136 $m^2\cdot g^{-1}$, and the highest surface oxygen content (31.98%). $Ce_{1-x}Mg_xO_2$ catalytic material was coated on the cordierite honeycomb ceramic to make a monolithic catalyst, and its catalytic performance for the direct synthesis of dimethyl carbonate from CO_2 and CH_3OH was investigated. Under the conditions of 140 ℃, 2.4 MPa, and 2 h reaction, the yield of dimethyl carbonate on $Ce_{0.90}Mg_{0.10}O_2$ monolith catalyst was as high as 20.21%, and the catalytic

收稿日期:2022-03-17。收修改稿日期:2022-05-18。

国家自然科学基金(No.21773189)、四川省中央引导地方科技发展专项(No.2021ZYD0044)、四川省科技厅项目(No.19ZDZX0113)和西南石油大学科研启动项目(No.2021QHZ023)资助。

*通信联系人。E-mail:yongdongchen@swpu.edu.cn,tana@dicp.ac.cn

activity was significantly higher than that of CeO_2 and other $Ce_{1-x}Mg_xO_2$ (x=0.05, 0.15, 0.20) catalytic materials.

Keywords: CO_2 conversion; dimethyl carbonate; oxygen vacancies; monolithic catalyst; magnesium-cerium oxides

0 Introduction

Dimethyl carbonate (DMC) has been widely applied as a fuel additive, in electrochemistry and organic synthesis due to its environmental-friendly properties[1-3]. Although many methods have been applied for DMC synthesis, such as phosgene method, transesterification method, urea alcoholysis method, epoxy alkane method, methanol, and CO_2 direct synthesis method, *etc*.[4-6]. Direct synthesis of DMC from CO_2 and methanol has attracted great attention (Scheme 1)[7]. The utilization of CO_2 as the carbon source instead of fossil feedstock may promote the sustainability of the chemical industry and terminate the greenhouse effect caused by excessive CO_2 emission. However, there are still some vital challenges such as low yield, deactivation of the catalyst, and thermodynamic limitations for this route[6,8]. Thus, designing novel catalysts and developing efficient water removing methods from the reaction mixture are crucial to overcoming the thermodynamic equilibrium of the reaction.

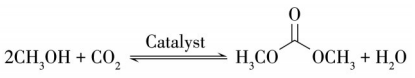

Scheme 1　Direct synthesis of DMC from CO_2 and methanol

Ceria-based nanomaterials have been widely studied in the direct synthesis of DMC from CO_2 and methanol. This is mainly due to its fascinating CO_2 capture ability which significantly affects the reaction efficiency. Inert CO_2 molecular in the gas phase needs to be adsorbed and activated by the surface oxygen vacancy sites and then can react with methanol to generate DMC[9-12]. Doping metal ions while maintaining the fluorite crystalline structure of ceria is one of the effective ways to enhance the concentration of surface oxygen vacancy of CeO_2[9,13-14]. Because the impurity ions can reduce the crystalline size, generate more surface defects and boost the reducibility of surface oxygen[15-16]. On another hand, the surface acid - base property of CeO_2 can be mediated by the doping method, which will further favor the formation of DMC to improve the selectivity[9]. According to Scheme 1, the reaction equilibrium can shift toward the right side by water removal[17]. Usually, inorganic dehydrating agents are introduced to physically remove water with limited effect due to the low dehydration capacity at reaction temperatures[18-21]. While organic dehydrating agents are applied to remove water by chemical reactions which may form lots of by-products complicating the entire process[22-25]. Coating the catalyst powder on the surface of cordierite honeycomb ceramics can improve the phase-phase mass transfer performance[26-28]. Therefore, it is reasonable to expect an enhanced efficiency for water removal using a honeycomb structure catalyst, which will improve the DMC yield in return.

In this contribution, $Ce_{1-x}Mg_xO_2$ (x=0.05, 0.10, 0.15, 0.20) solid solutions with a variation of magnesium content were prepared by the co-precipitation method to find an optimal ratio. Mg ions doping in CeO_2 lattice adjusted the surface acid-base property and the surface oxygen vacancies. Among all the obtained catalytic materials, $Ce_{0.90}Mg_{0.10}O_2$ was found to show the best catalytic activity in the direct synthesis of DMC from methanol and carbon dioxide. Using a unique structure, monolithic catalyst produced by coating powder on cordierite honeycomb ceramics showed high effective and stable catalytic performance. At 140 ℃, 2.4 MPa, and 2 h continuous reaction, the yield of DMC over $Ce_{0.90}Mg_{0.10}O_2$ monolithic catalyst was the highest (20.21%).

1 Experimental

1.1 Materials preparations

The preparation of $Ce_{0.90}Mg_{0.10}O_2$ by the co-precipitation method is described as an example. We weighed 15.000 0 g $(NH_4)_2Ce(NO_3)_6$, 0.779 5 g $Mg(NO_3)_2 \cdot 6H_2O$, and 70.000 0 g urea (CH_4N_2O) and dissolved them completely with 500 mL deionized water under

stirring. The mixture was transferred to a 1 000 mL three-neck flask and gradually heated to 90 ℃ under mechanical stirring (600 r·min^{-1}) for 5 h. After the reaction, the product was cooled to room temperature naturally, the precipitate was filtered and washed with water (over 4 000 mL) and absolute ethanol (about 300 mL), dried overnight at 80 ℃, and calcined at 400 ℃ for 4 h in the air to obtain the target product. The obtained $Ce_{1-x}Mg_xO_2$ powder was ground with the required deionized water to obtain a slurry, which was coated on a cordierite honeycomb ceramics (64 cells per cm^2, Φ: 10 mm, L: 25 mm). The load was maintained at 0.5 g, and the excess slurry was blown away. Finally, the coated catalyst was dried overnight at 80 ℃ and calcined at 400 ℃ for 4 h in the air to obtain a $Ce_{0.90}Mg_{0.10}O_2$ monolithic catalyst. The preparation method of $Ce_{0.95}Mg_{0.05}O_2$, $Ce_{0.85}Mg_{0.15}O_2$, and $Ce_{0.80}Mg_{0.20}O_2$ monolithic catalysts were the same as above, only the mass of $Mg(NO_3)_2·6H_2O$ was changed.

1.2 Catalytic tests

The catalytic activity of the prepared catalyst for the direct synthesis of DMC from CO_2 and methanol was evaluated in a continuous fixed-bed reactor. Water was the main disadvantageous factor for the formation of DMC in the synthesis reaction. The flow of the reaction system can remove the water vapor well and detect the reaction products online. A typical procedure was to place the prepared $Ce_{1-x}Mg_xO_2$ monolith catalyst in a stainless steel reaction tube. The reactor was sealed and purged with a CO_2 stream for 30 min to drain the internal air. When the reaction system reached the required temperature, a mixed gas stream of CH_3OH (0.145 mL·min^{-1}) and CO_2 (40 mL·min^{-1}) (n_{CH_3OH}: n_{CO_2}= 2∶1) was introduced. Then the reaction was carried out at 140 ℃, 2.4 MPa, and 2 880 h^{-1} of gas hourly space velocity (GHSV). The outlet component after the reaction was analyzed online using gas chromatography (Agilent 7890B) equipped with a hydrogen flame ionization detector. The calculation formula for CH_3OH conversion and DMC selectivity is as follows:

$$\text{Conversion} = \frac{2c_{DMC} + c_{HCHO} + 2c_{DME}}{c_{CH_3OH} + 2c_{DMC} + 2c_{DME} + c_{HCHO}} \times 100\% \quad (1)$$

$$\text{Selectivity} = \frac{c_{DMC}}{c_{DMC} + c_{DME} + c_{HCHO} + c_{CO}} \times 100\% \quad (2)$$

Where c_i represents the concentration of a component (i).

2 Results and discussion

2.1 Characterization of as-prepared solid solutions

Fig.1 shows the X-ray diffraction (XRD) patterns of the prepared $Ce_{1-x}Mg_xO_2$ composite oxides (Detailed characterization conditions can be found in Supporting Information). CeO_2 samples showed typical diffraction lines of cubic fluorite structure (PDF No. 43-1002). Besides, it can be seen that the catalyst doped with Mg^{2+} still maintained the characteristic peak of cubic fluorite ceria after calcination, no diffraction line representing MgO or any other impurities was detected. Compared with pure CeO_2, the (111) plane peak shifted to a higher angle with increased Mg concentration (Fig.1b), indicating a lattice contraction. The calculated lattice constant decreased from 0.541 8 nm for CeO_2 to 0.540 6 nm for $Ce_{0.80}Mg_{0.20}O_2$ (Table 1) because the ionic radius of Mg^{2+} (0.089 nm) is smaller than that of Ce^{4+} (0.097 nm). The XRD patterns imply that the Mg^{2+} incorporate into the CeO_2 lattice forming no MgO species and part of them substitutes the Ce^{4+} leading to lattice contraction. These results are in good agreement with previous reports[15,29-30]. The calculated grain size from (111) for all samples ranges from 5.8 to 6.1 nm and the specific surface area is basically the same, indicating that the addition of Mg has little influence on the micro-textural property.

The N_2 adsorption-desorption isotherms and pore size distributions of $Ce_{1-x}Mg_xO_2$ catalyst are shown in Fig.S1. As shown in Fig.S1, all catalysts obtained type

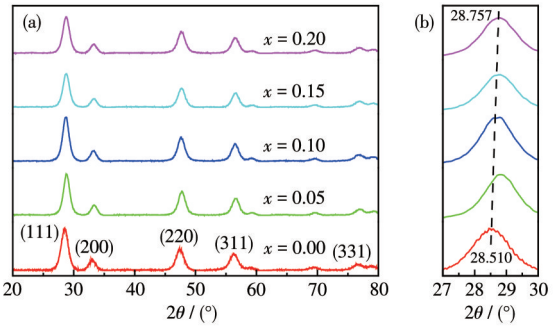

Fig.1 (a) XRD patterns of $Ce_{1-x}Mg_xO_2$ composite oxides and (b) zoomed-in view of the (111) plane peak

Ⅳ isotherms with clear H3 hysteresis lines, indicating typical mesoporous materials. In Fig. S2, all catalysts contain mesopore pore size distributions with pore sizes ranging from 2 to 20 nm. The above results show that the Mg^{2+} content has a significant effect on the pore size distribution. The BET (Brunauer - Emmett - Teller) surface area and pore volume of the synthesized $Ce_{1-x}Mg_xO_2$ catalyst are summarized in Table 1. It can be observed that $Ce_{0.90}Mg_{0.10}O_2$ composite oxide possesses the highest specific surface area of 136 $m^2 \cdot g^{-1}$ and pore volume of 0.188 $cm^3 \cdot g^{-1}$.

Transmission electron microscope (TEM) images (Fig.2) of as-prepared $Ce_{1-x}Mg_xO_2$ composite oxides indicated that all samples were in irregular spherical shape exposing no specific facets. The average particle size of as-prepared $Ce_{1-x}Mg_xO_2$ is consistent with the grain size.

There are two bands observed in Raman spectra (Fig. 3). The vibration peak around 461 cm^{-1} can be attributed to the F_{2g} vibrational mode of Ce—O, which usually shows a sharp and symmetric band at 466 cm^{-1} [9,31]. Considering the high specific surface area of the prepared material, the peak shifted to low frequency and showed asymmetric character, which are mainly attributed to the small particle size. Compared with as-prepared CeO_2 nanoparticles, the F_{2g} band gradually blue-shifted with increased Mg^{2+} content, which demonstrates the decreased average length of Ce—O bond

Table 1　Structural and textural properties of $Ce_{1-x}Mg_xO_2$ composite oxides

Catalyst	(111) plane		Lattice parameter[a] / nm	Particle size[b] / nm	S_{BET} / ($m^2 \cdot g^{-1}$)	V_{Pore} / ($m^3 \cdot g^{-1}$)
	2θ / (°)	d / nm				
CeO_2	28.510	0.312 8	0.541 8	8.6	133	0.131
$Ce_{0.95}Mg_{0.05}O_2$	28.709	0.311 3	0.540 5	6.7	129	0.142
$Ce_{0.90}Mg_{0.10}O_2$	28.730	0.310 0	0.540 1	5.8	136	0.188
$Ce_{0.85}Mg_{0.15}O_2$	28.770	0.310 1	0.539 8	6.1	117	0.129
$Ce_{0.80}Mg_{0.20}O_2$	28.757	0.310 2	0.540 6	6.3	126	0.168

[a] Calculated using Vegard's law; [b] Estimated by TEM.

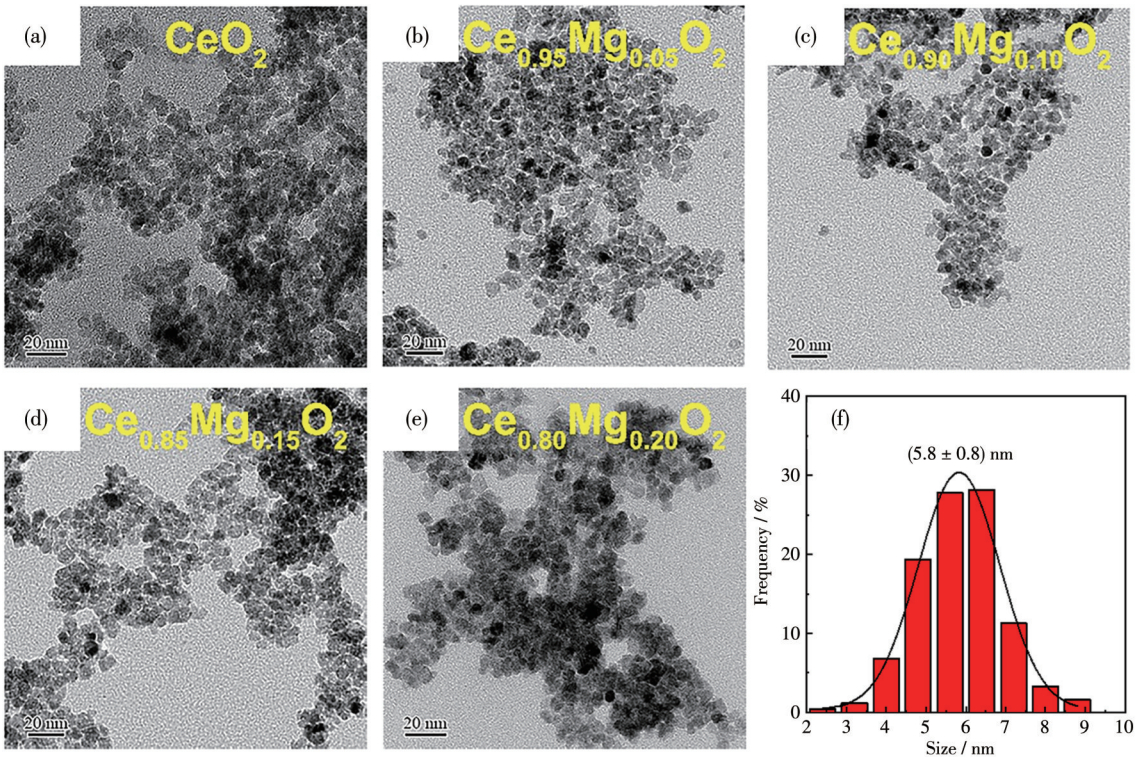

Fig.2　(a-e) TEM images of $Ce_{1-x}Mg_xO_2$ composite oxides; (f) Size distribution of $Ce_{0.90}Mg_{0.10}O_2$

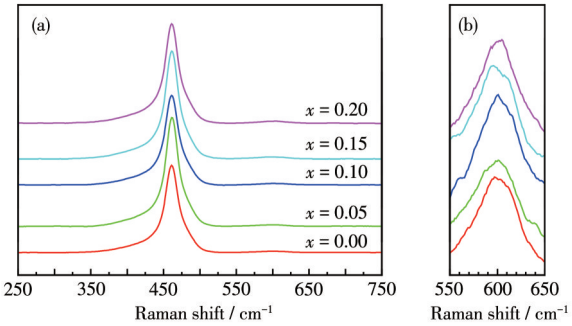

Fig.3 (a) Raman spectra of $Ce_{1-x}Mg_xO_2$ composite oxides and (b) zoomed-in view of the peak attributed to oxygen vacancies

and lattice contraction further. Therefore, it is reasonable to deduce that smaller Mg^{2+} cations substitute some Ce^{4+} ions in the fluorite lattice. It is also noted that the intensity of F_{2g} decreased with increased Mg^{2+} content, revealing structural distortion[32-33]. Another band near 596 cm^{-1} is related to the oxygen vacancies caused by the Ce^{3+} ion in the CeO_2 lattice (Fig. 3b)[34]. The intensity of this mode increased with an increase of Mg^{2+} content, pointing at increased intrinsic oxygen vacancy concentration. No Raman shifts of MgO were observed in $Ce_{1-x}Mg_xO_2$, which further infers $Ce_{1-x}Mg_xO_2$ prefers a solid solution state.

To elaborate on changes in the CeO_2 chemical state after Mg doping, X-ray photoelectron spectroscopy (XPS) analysis was carried out. The XPS spectra of Ce3*d* (Fig. 4a) exhibit complex features with eight peaks. U and V represent spin-orbits of Ce3$d_{3/2}$ and Ce3$d_{5/2}$, respectively. Spin-orbit doublet (V‴ *ca.* 898.3 eV and U‴ *ca.* 916.8 eV, V″ *ca.* 888.9 eV and U″ *ca.* 907.4 eV, V *ca.* 882.4 eV and U *ca.* 900.9 eV) are attributed to the Ce^{4+} species, while (V′ *ca.* 884.9 eV and U′ *ca.* 903.4 eV) are assigned to the Ce^{3+} species[29,31]. Then the concentration of Ce^{3+} can be estimated by taking the ratio of the area of the integrated peak corresponding to Ce^{3+} to the total area of fitted peaks. It is shown that Mg doping has enhanced the concentration of Ce^{3+} on the surface remarkably, and the maximum ratio (19.42%) has been obtained when 10% Mg doping. The O1*s* XPS spectra (Fig. 4b) of $Ce_{1-x}Mg_xO_2$ composite oxides can be deconvoluted into 3 surface oxygen species: lattice oxygen (O_L *ca.* 529.3 eV), surface oxygen vacancies (O_V *ca.* 530.5 eV); and chemisorption oxygen species (O_C) at the highest binding energy (*ca.* 532.2 eV)[35]. The intensity ratio of surface oxygen vacancies to the sum of all oxygen species was summarized in Table 2. It was observed that the incorporation of Mg^{2+} can effectively increase the number of surface oxygen species (O_V+O_C). These results confirm that there are enhanced mobility and availability of lattice oxygen species due to the synergistic effect between MgO and CeO_2.

Fig. 5 shows the temperature-programmed reduction by hydrogen (H_2-TPR) profile of as-prepared $Ce_{1-x}Mg_xO_2$ composite oxides. The TPR of pure CeO_2 showed a broad peak starting at 500 ℃ and one peak at 825 ℃, representing the surface and the bulk reduction process, respectively. The surface reduction initiated around a lower temperature 500 ℃ after Mg^{2+} ions (less than 20%) were introduced, which means the reducibility of surface oxygen species has been significantly improved. Meanwhile, the area of this broad peak increased gradually with higher Mg concentration as well, indicating the lattice oxygen in bulk can move to

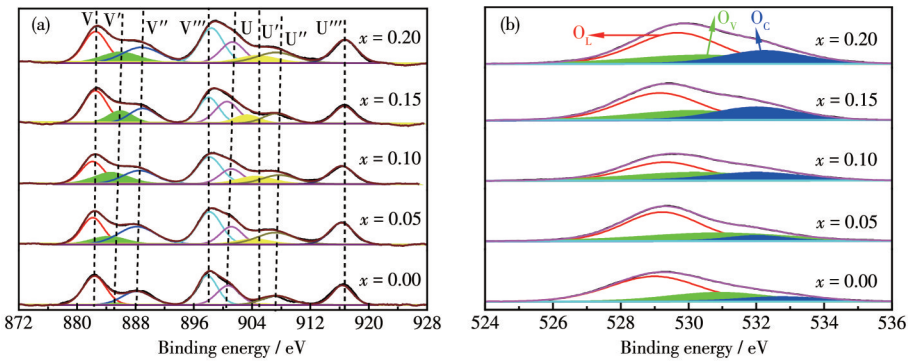

Fig.4 (a) Ce3*d* and (b) O1*s* XPS spectra of $Ce_{1-x}Mg_xO_2$ composite oxides

Table 2　Relative ratio of Ce^{3+} species and oxygen vacancies on the surface

Catalyst	Surface content of Ce^{3+} / %	Surface content of O_V+O_C / %	Total amount of adsorbed CO_2[a] / ($mmol_{CO_2}\cdot g_{cat}^{-1}$)
CeO_2	1.34	24.97	0.787
$Ce_{0.95}Mg_{0.05}O_2$	11.57	30.85	0.794
$Ce_{0.90}Mg_{0.10}O_2$	19.42	31.98	0.845
$Ce_{0.85}Mg_{0.15}O_2$	15.18	25.06	0.808
$Ce_{0.80}Mg_{0.20}O_2$	15.40	23.19	0.771

[a] Determined using the CO_2 temperature-programmed desorption (CO_2-TPD) analysis in Fig.S3.

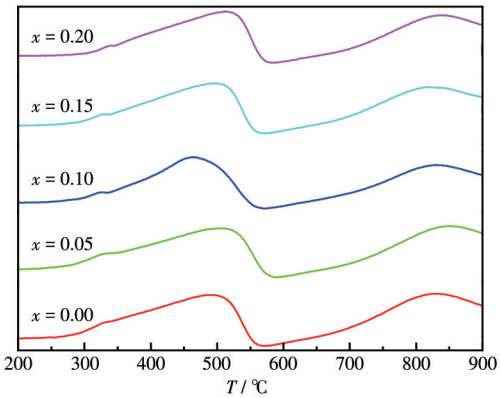

Fig.5　H_2-TPR profiles of CeO_2 and $Ce_{1-x}Mg_xO_2$ composite oxides

the surface and participate in chemical reactions at a relatively lower temperature. Thus not only the reducibility of surface oxygen but also the mobility of lattice have activated due to Mg^{2+} introduction, resulting in more oxygen vacancies, probably by reducing the interaction between Ce—O with a distorted crystalline structure. This feature will facilitate chemical reactions whose reactants would be activated by oxygen vacancies. According to the related literature, the oxygen vacancy is crucial for activating carbon dioxide in the direct synthesis of DMC from CO_2 and methanol[11,34,36].

2.2　Catalytic performance

Fig. 6a illustrates photographs of as-prepared monolithic catalyst. A scanning electron microscope (SEM) image (Fig. 6) revealed that the average thickness of the catalyst coating was *ca*. 60 μm. Well uniform coating layers were found, as evidenced in the corner, inner, and frontal channel views from the energy dispersion X-ray spectrum (EDS) mappings of $Ce_{0.90}Mg_{0.10}O_2$-coated monolithic catalyst. The abnormal distribution of Mg is due to a small amount of Mg in cordierite. It also demonstrates that $Ce_{0.90}Mg_{0.10}O_2$-coated monolithic catalyst can be insufficient contact with the reaction gas stream to promote the conversion and the yield of the product[37]. Catalyst activity of monolithic and particulate (40-60 mesh) $Ce_{0.90}Mg_{0.10}O_2$ catalyst was comparatively studied (Fig.7). It is easy to conclude this monolithic do have enhanced the DMC yield and methanol conversion even though both were carried out in the same fixed bed reactor. Therefore, it

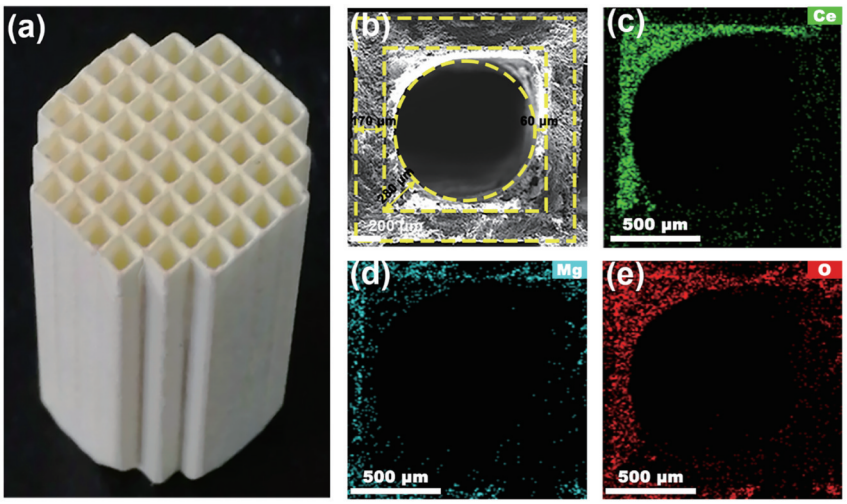

Fig.6　(a) Photographs, (b) SEM image, and (c-e) EDS element mappings on $Ce_{0.90}Mg_{0.10}O_2$-coated monolithic catalyst

is probable that the unique structure of the monolithic catalyst accelerates the water removal and shifts the reaction equilibrium successfully. Fig.8 shows the performance of $Ce_{1-x}Mg_xO_2$ monolithic catalysts on direct DMC synthesis. The optimum temperature and optimum pressure can be obtained from Fig.S4 and S5. The activity of the catalyst was $Ce_{0.90}Mg_{0.10}O_2$> $Ce_{0.95}Mg_{0.05}O_2$> CeO_2> $Ce_{0.85}Mg_{0.15}O_2$> $Ce_{0.80}Mg_{0.20}O_2$. When x=0.10, the yield of DMC reached the maximum of 20.21% and decreased with a higher doping concentration. It is mainly reflected in the decrease of DMC selectivity and the increase of HCHO and DME selectivity.

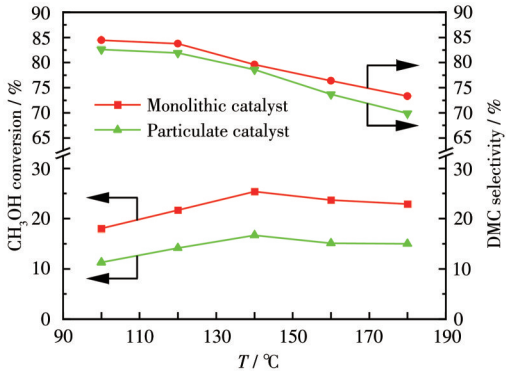

Fig.7 Catalytic activity of monolithic and particulate $Ce_{0.90}Mg_{0.10}O_2$ catalyst

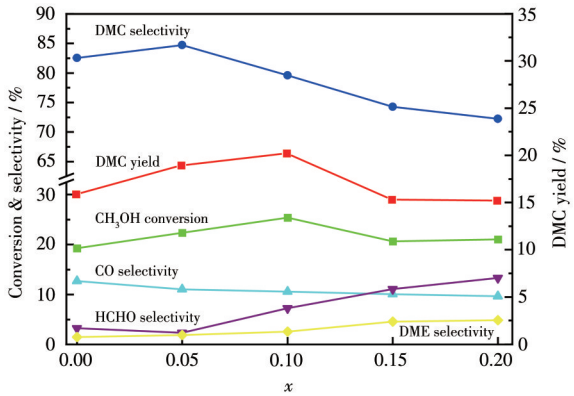

Reaction conditions: catalyst: 500 mg, GHSV: 2 880 mL·g_{cat}^{-1}·h^{-1}, n_{CH_3OH}:n_{CO_2}=2:1, temperature: 140 ℃, pressure: 2.4 MPa

Fig.8 Catalytic performance of $Ce_{1-x}Mg_xO_2$ monolithic catalysts

According to our previous studies, there are the following reaction processes in this process: (Ⅰ) $2CH_3OH \rightarrow CH_3OCH_3+H_2O$; (Ⅱ) $2CH_3O+CO_2 \rightarrow HCHO+CO+H_2O$[35]. It can be seen that the doping of Mg can promote the process of (Ⅰ) and (Ⅱ), which leads to a decrease in the selectivity of DMC.

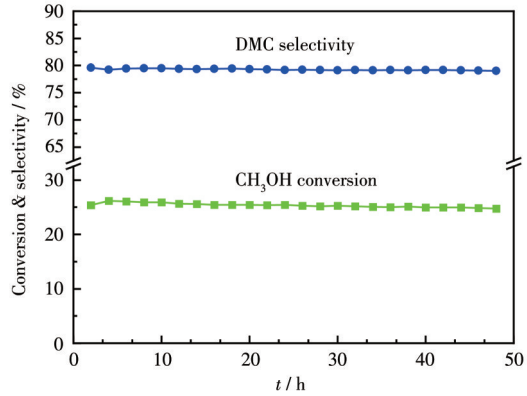

Reaction conditions: catalyst: 500 mg, GHSV: 2 880 mL·g_{cat}^{-1}·h^{-1}, n_{CH_3OH}:n_{CO_2}=2:1, temperature: 140 ℃, pressure: 2.4 MPa

Fig.9 Durability test of $Ce_{0.90}Mg_{0.10}O_2$ monolithic catalyst

To provide referable information for the industry, we examined the stability of $Ce_{0.90}Mg_{0.10}O_2$ monolithic catalyst at 140 ℃ and 2.4 MPa. There is little deactivation for this catalyst (DMC yield from 20.21% to 19.56%) during the 50 h durability test implies it is a quite promising application for the direct synthesis of DMC from CO_2 and methanol.

3 Conclusions

In conclusion, doping Mg in CeO_2 lattice can enhance the catalytic performance on the direct formation of DMC from methanol and CO_2. Since Mg^{2+} ions play an important role in the activation of oxygen species in CeO_2 lattice, which favors the oxygen vacancies formation. At the same time, the honeycomb structure of the monolithic catalyst greatly improves the removal of reaction products, overcoming thermodynamic limitations to some extent. Consequently, the yield of DMC and the stability of the catalyst can be improved.

Supporting information is available at http://www.wjhxxb.cn

Acknowledgments: We acknowledge XIAO Yong - Li, JIANG Lan for their aid in this work.

References:

[1]Schifter I, Gonzalez U, Gonzalez-Macias C. Effects of Ethanol, Ethyl-*tert*-butyl Ether and Dimethyl Carbonate Blends with Gasoline on SI engine. *Fuel*, **2016**,**183**:253-261

[2]Tundo P, Musolino M, Aricò F. The Reactions of Dimethyl Carbonate

and Its Derivatives. *Green Chem.*, **2018**,**20**:28-85

[3]Selva M, Perosa A, Fiorani G. Dimethyl Carbonate: A Versatile Reagent for a Sustainable Valorization of Renewables. *Green Chem.*, **2018**,**20**: 288-322

[4]Keller N, Rebmann G, Keller V. Catalysts, Mechanisms and Industrial Processes for the Dimethyl Carbonate Synthesis. *J. Mol. Catal. A: Chem.*, **2010**,**317**:1-18

[5]Saavalainen P, Kabra S, Turpeinen E, Oravisjärvi K, Yadav G D, Keiski R L, Pongrácz E. Sustainability Assessment of Chemical Processes: Evaluation of Three Synthesis Routes of DMC. *J. Chem.*, **2015**: 1-12

[6]Tamboli A H, Chaugule A A, Kim H. Catalytic Developments in the Direct Dimethyl Carbonate Synthesis from Carbon Dioxide and Methanol. *Chem. Eng. J.*, **2017**,**323**:530-544

[7]Dabral S, Schaub T. The Use of Carbon Dioxide (CO_2) as a Building Block in Organic Synthesis from an Industrial Perspective. *Adv. Synth. Catal.*, **2019**,**361**:223-246

[8]Cai Q H, Lu B, Guo L J, Shan Y K. Studies on Synthesis of Dimethyl Carbonate from Methanol and Carbon Dioxide. *Catal. Commun.*, **2009**, **10**:605-609

[9]Liu B, Li C M, Zhang G Q, Yan L F, Li Z. Direct Synthesis of Dimethyl Carbonate from CO_2 and Methanol over CaO - CeO_2 Catalysts: The Role of Acidic-Basic Properties and Surface Oxygen Vacancies. *New J. Chem.*, **2017**,**41**:12231-12240

[10]Marciniaka A A, Henriqueb F J F S, Limac A F F, Alvesd O C, Moreirae C R, Appele L G, Mota C J A. What are the Preferred CeO_2 Exposed Planes for the Synthesis of Dimethyl Carbonate? Answers from Theory and Experiments. *Mol. Catal.*, **2020**,**493**:111053

[11]Fu Z W, Yu Y H, Li Z, Han D M, Wang S J, Xiao M, Meng Y Z. Surface Reduced CeO_2 Nanowires for Direct Conversion of CO_2 and Methanol to Dimethyl Carbonate: Catalytic Performance and Role of Oxygen Vacancy. *Catalysts*, **2018**,**8**:164

[12]Zhao S Y, Wang S P, Zhao Y J, Ma X B. An *In Situ* Infrared Study of Dimethyl Carbonate Synthesis from Carbon Dioxide and Methanol over Well-Shaped CeO_2. *Chin. Chem. Lett.*, **2017**,**28**:65-69

[13]Tamboli A H, Chaugule A A, Gosavi S W, Kim H. $Ce_xZr_{1-x}O_2$ Solid Solutions for Catalytic Synthesis of Dimethyl Carbonate from CO_2: Reaction Mechanism and the Effect of Catalyst Morphology on Catalytic Activity. *Fuel*, **2018**,**216**:245-254

[14]Fu Z W, Zhong Y Y, Yu Y H, Long L Z, Xiao M, Han D M, Wang S J, Meng Y Z. TiO_2-Doped CeO_2 Nanorod Catalyst for Direct Conversion of CO_2 and CH_3OH to Dimethyl Carbonate: Catalytic Performance and Kinetic Study. *ACS Omega*, **2018**,**3**:198-207

[15]Yu Q, Wu X X, Tang C J, Qi L, Liu B, Gao F, Sun K Q, Dong L, Chen Y. Textural, Structural, and Morphological Characterizations and Catalytic Activity of Nanosized CeO_2-MO_x (M=Mg^{2+}, Al^{3+}, Si^{4+}) Mixed Oxides for CO Oxidation. *J. Colloid Interface Sci.*, **2011**,**354**: 341-352

[16]Kang K H, Joe W, Lee C H, Kim M, Kim D B, Jang B, Song I K. Direct Synthesis of Dimethyl Carbonate from Methanol and Carbon Dioxide Over $CeO_2(X)$-ZnO(1−X) Nano-Catalysts. *J. Nanosci. Nanotechnol.*, **2013**,**13**:8116-8120

[17]Sakakura T, Choi J, Saito Y, Sako T. Synthesis of Dimethyl Carbonate from Carbon Dioxide: Catalysis and Mechanism. *Polyhedron*, **2000**,**19**:573-576

[18]Honda M, Tamura M, Nakagawa Y, Nakao K, Suzuki K, Tomishige K. Organic Carbonate Synthesis from CO_2 and Alcohol over CeO_2 with 2 - Cyanopyridine: Scope and Mechanistic Studies. *J. Catal.*, **2014**,**318**:95-107

[19]Stoian D, Medina F, Urakawa A. Improving the Stability of CeO_2 Catalyst by Rare Earth Metal Promotion and Molecular Insights in the Dimethyl Carbonate Synthesis from CO_2 and Methanol with 2-Cyanopyridine. *ACS Catal.*, **2018**,**8**:3181-3225

[20]Wang S P, Zhou J J, Zhao S Y, Zhao Y J, Ma X B. Enhancements of Dimethyl Carbonate Synthesis from Methanol and Carbon Dioxide: The *In Situ* Hydrolysis of 2-Cyanopyridine and Crystal Face Effect of Ceria. *Chin. Chem. Lett.*, **2015**,**26**:1096-1100

[21]Sakakura T, Saito Y, Okano M, Choi J C, Sako T. Selective Conversion of Carbon Dioxide to Dimethyl Carbonate by Molecular Catalysis. *J. Org. Chem.*, **1998**,**63**:7095-7096

[22]Marciniak A A, Alves O C, Appel L G, Mota C J A. Synthesis of Dimethyl Carbonate from CO_2 and Methanol over CeO_2: Role of Copper as Dopant and the Use of Methyl Trichloroacetate as Dehydrating Agent. *J. Catal.*, **2019**,**371**:88-95

[23]Bansode A, Urakawa A. Continuous DMC Synthesis from CO_2 and Methanol over a CeO_2 Catalyst in a Fixed Bed Reactor in the Presence of a Dehydrating Agent. *ACS Catal.*, **2014**,**4**:3877-3880

[24]Han D M, Chen Y, Wang S J, Xiao M, Lu Y X, Meng Y Z. Effect of Alkali - Doping on the Performance of Diatomite Supported Cu - Ni Bimetal Catalysts for Direct Synthesis of Dimethyl Carbonate. *Catalysts*, **2018**,**8**:302-312

[25]Santos B, Silva V, Loureiro J, Rodrigues A E. Adsorption of H_2O and Dimethyl Carbonate at High Pressure over Zeolite 3A in Fixed Bed Column. *Ind. Eng. Chem. Res.*, **2014**,**53**:2473-2483

[26]Chen Y D, Yang Y, Tian S L, Ye Z B, Li G. Highly Effective Synthesis of Dimethyl Carbonate over CuNi Alloy Nanoparticles@Porous Organic Polymers Composite. *Appl. Catal. A*, **2019**,**587**:117275

[27]Vita A, Italiano C, Pino L, Frontera P, Ferraro M, Antonucci V. Activity and Stability of Powder and Monolith-Coated Ni/GDC Catalysts for CO_2 Methanation. *Appl. Catal. B*, **2018**,**226**:384-395

[28]Tsa S B, Ma H. A Research on Preparation and Application of the Monolithic Catalyst with Interconnecting Pore Structure. *Sci. Rep.*, **2018**,**8**:16605

[29]Jin S, Bang G, Liu L, Lee C H. Synthesis of Mesoporous MgO-CeO_2 Composites with Enhanced CO_2 Capture Rate via Controlled Combustion. *Microporous Mesoporous Mater.*, **2019**,**288**:109587

[30]Matović B, Luković J, Stojadinović B, Aškrabić S, Zarubica A, Babić B, Dohčević-Mitrović Z. Influence of Mg doping on Structural, Optical and Photocatalytic Performances of Ceria Nanopowders. *Process. Appl. Ceram.*, **2017**,**11**:304-310

[31]Liu H, Zou W J, Xu X L, Zhang X L, Yang Y Q, Tian G, Feng S H. The Proportion of Ce^{4+} in Surface of $Ce_xZr_{1-x}O_2$ Catalysts: The Key

Parameter for Direct Carboxylation of Methanol to Dimethyl Carbonate. *J. CO_2 Util.*, **2017**,**17**:43-49

[32]Alla S K, Mandal R K, Prasad N K. Optical and Magnetic Properties of Mg^{2+} Doped CeO_2 Nanoparticles. *RSC Adv.*, **2016**, **6**: 103491 - 103498

[33]Ma X, Lu P, Wu P. Structural, Optical and Magnetic Properties of CeO_2 Nanowires with Nonmagnetic Mg^{2+} Doping. *J. Alloys Compd.*, **2017**,**734**:22-28

[34]Liu B, Li C M, Zhang G, Yao X, Chuang S, Li Z. Oxygen Vacancy Promoting Dimethyl Carbonate Synthesis from CO_2 and Methanol over Zr-Doped CeO_2 Nanorods. *ACS Catal.*, **2018**,**8**:10446-10473

[35]Chen Y D, Wang H, Qin Z, Tian S, Li G. $Ti_xCe_{1-x}O_2$ Nanocomposites: A Monolithic Catalyst for Direct Conversion of Carbon Dioxide and Methanol to Dimethyl Carbonate. *Green Chem.*, **2019**,**21**:4642-4649

[36]Pu Y F, Xuan K, Wang F, Li A X, Zhao N, Xiao F K. Synthesis of Dimethyl Carbonate from CO_2 and Methanol over a Hydrophobic Ce/SBA-15 Catalyst. *RSC Adv.*, **2018**,**8**:27216-27226

[37]Bustamante F, Orrego A F, Villegas S, Villa A L. Modeling of Chemical Equilibrium and Gas Phase Behavior for the Direct Synthesis of Dimethyl Carbonate from CO_2 and Methanol. *Ind. Eng. Chem. Res.*, **2012**,**51**:8945-8956